Articles in PresS. J Neurophysiol (July 13, 2011). doi:10.1152/jn.00104.2011

Neural decoding of treadmill walking from non-invasive, electroencephalographic (EEG) signals

Alessandro Presacco[1], Ronald Goodman[5], Larry Forrester[4,5] and Jose Luis Contreras-Vidal[1,2,3]

University of Maryland, College Park:

[1]Neural Engineering and Smart Prosthetics Research Laboratory, Department of Kinesiology, School of Public Health

[2]Fischell Department of Bioengineering

[3]Graduate Program in Neuroscience and Cognitive Science;

University of Maryland, Baltimore:

[4]Department of Physical Therapy & Rehabilitation Science, University of Maryland School of Medicine

[5]Veteran Affairs Medical Center, Baltimore

Author Contributions: JLCV conceived the research; JLCV designed the experiment with assistance from LF; AP, LF and RG performed the research at the VAMC; AP and JLCV designed the decoders, and analyzed the data at UMCP; AP and JLCV wrote the paper; and LF and RG edited the manuscript.

Correspondence to:

Alessandro Presacco or Jose L. Contreras-Vidal

School of Public Health, Department of Kinesiology

SPH Building, University of Maryland, College Park

College Park, MD 20742

Tel: (305) 496 5457, Email: {apresacc@umd.edu; pepeum@umd.edu}

Abstract

Chronic recordings from ensembles of cortical neurons in primary motor and somatosensory areas in rhesus macaques provide accurate information about bipedal locomotion (Fitzsimmons et al. 2009). Here we show that the linear and angular kinematics of the ankle, knee and hip joints during both normal and precision (attentive) human treadmill walking can be inferred from noninvasive scalp electroencephalography (EEG) with decoding accuracies comparable to those from neural decoders based on multiple single-unit activity (SUAs) recorded in nonhuman primates. Six healthy adults were recorded. Participants were asked to walk on a treadmill at their self-selected comfortable speed while receiving visual feedback of their lower limbs (i.e., precision walking), to repeatedly avoid stepping on a strip drawn on the treadmill belt. Angular kinematics of the left and right hip, knee and ankle joints and EEG were recorded, and neural decoders were designed and optimized using cross-validation procedures. Of note, these decoders were also used to accurately infer gait trajectories in a normal walking task that did not require subjects to control and monitor their foot placement. Our results indicate a high involvement of a fronto-posterior cortical network in the control of both precision and normal walking and suggest that EEG signals can be used to study in real-time the cortical dynamics of walking and to develop brain-machine interfaces aimed at restoring human gait function.

Key Words: BCI; BMI; EEG; neural decoding; treadmill; walking

Introduction

Little is known about the organization, neural network mechanisms and computations underlying the control of walking in humans (Choi and Bastian 2007). Although central pattern generators for locomotion are important in the control of walking, supra-spinal networks, including the brainstem, cerebellum and cortex, must be critical as demonstrated by the changing motor and cognitive (i.e., spatial attention) demands imposed by bipedal walking in unknown or cluttered dynamic environments (Choi and Bastian 2007; Grillner et al. 2008; Nielsen 2003; Rossignol et al. 2007). Neuroimaging studies show that rhythmic foot or leg movements recruit primary motor cortex (Christensen et al. 2001; Dobkin et al. 2004; Heuninckx et al. 2005; Heuninckx et al. 2008; Luft et al. 2002; Sahyoun et al. 2004), whereas electrophysiological investigations demonstrate electrocortical potentials related to lower limb movements (Wieser et al. 2010), as well as a greater involvement of human cortex during steady-speed locomotion than previously thought (Gwin et al. 2010a, 2010b). In this regard, studies using functional near-infrared spectroscopy (fNIRS) show involvement of frontal, premotor and supplementary motor areas during walking (Harada et al. 2009; Miyai et al. 2001; Suzuki et al. 2008; Suzuki et al. 2004). That primary sensorimotor cortices carry information about bipedal locomotion has been directly proven by the work of Nicolelis and colleagues (Fitzsimmons et al. 2009), who demonstrated that chronic recordings from ensembles of cortical neurons in primary motor (M1) and primary somatosensory (S1) cortices can be used to predict the kinematics of bipedal walking in rhesus macaques. However, neural decoding of bipedal locomotion in humans has not yet been demonstrated. Here we compare the predictive power of neural decoders based on human scalp (noninvasive) EEG signals during treadmill walking with that reported from multiple single unit activity (SUA) in the rhesus monkey performing bipedal treadmill walking (Fitzsimmons et al. 2009). We demonstrate the feasibility of using scalp EEG to reconstruct the detailed kinematics of human walking, and the potential of the proposed approach as a new tool for inferring the cortical contributions to walking.

Materials and Methods

Experimental setup and procedure. Six healthy adults, aged 18-45 (3 male, 3 female) with no history of neurological disease or lower limb pathology and free of injury participated in the study after giving informed consent. The study was conducted with approved protocols from the Institutional Review Boards at the University of Maryland College Park, the University of Maryland Baltimore, and the Baltimore VA Research and Development Committee.

Participants were first asked to walk on a treadmill, to establish their comfortable speed during a 5-minute familiarization period that preceded the beginning of the recordings. Next, a 2-minute rest period (baseline) while standing on the treadmill was followed by 5-minutes of *precision walking*, when subjects were instructed to walk on the treadmill at their comfortable speed while receiving real time visual feedback (30 frames/sec) of their lower limbs through a video monitor in front of them. Subjects were told to avoid stepping on the white stripe (2 inches wide) glued diagonally on the treadmill's belt by using the monitor's video to keep track of foot placement relative to the white stripe. This increased the attentional demands during treadmill walking (Yogev-Seligman et al. 2008), a condition that can be considered to mimic walking in a novel environment or under novel conditions (e.g., after brain injury). Thus, the precision walking paradigm puts us a step closer to the actual application where patients have impaired gait function and therefore would need to rely purely or significantly on effortful attentive conscious control of gait. In an ancillary task, a subset of the participants whose decoders showed the best and worst decoding performance in the precision walking task were also tested under normal walking conditions that did not require precise positioning of the feet nor monitoring of foot placement through a computer monitor (subjects were instructed to direct their gaze straight ahead).

Limb movement and EEG recordings. The three-dimensional (3D) joint kinematics of the hip, knee and ankle joints were recorded using an infrared optical motion capture system (Optotrak, Northern Digital, Ontario, Canada @ 100 Hz) with foot switch data (Koningsberg

111 Instrumentation, Pasadena, CA, @ 100 Hz). Precision manufactured 5 cm diameter disks
112 (Innovative Sports Training, Chicago, IL), each embedded with three infrared diodes that formed
113 an equilateral triangle (~3 cm sides), were affixed with adhesive and secured with foam wrap at
114 the second sacral vertebra (S-2) and on the thigh, shank, and foot segments of each lower limb. A
115 segmental model of the lower limbs was then determined by digitizing joint centers for the hip,
116 knee and ankle joints of each limb. Gait kinematics were derived from the model using motion
117 analysis software (Motion Monitor, Innovative Sports Training, Chicago, IL) and exported as
118 ascii files containing time histories of the X, Y & Z positions, joint angular positions and joint
119 angular velocities for the hip, knee and ankle joints of the right leg. Whole scalp 60-channel EEG
120 (Neuroscan Synamps2 RT, Compumedics USA, Charlotte, NC, USA) and electro-ocular activity
121 were recorded (sampling rate of 500 Hz; band-pass filtered from 0.1 to 100 Hz; right ear lobe
122 (A2) was used as a reference) and time-locked with the movement kinematics using the
123 footswitch signals.
124
125 *Power spectral density analysis.* The power spectral density (PSD) for the kinematic data and for
126 each channel of the EEG recorded during rest and during the walking task for the 6 subjects was
127 computed using the adaptive Thompson's multitaper method as implemented in Matlab's *pmtm*
128 function. The time-bandwidth product for the discrete prolate spheroidal sequences used was 4
129 and the frequency resolution 0.1 Hz. The confidence interval was set to 95% and was estimated
130 using a chi-squared approach. In order to account for the variability of the kinematics, and for
131 purposes of cross-validation of the decoders (see the *Model performance metrics* subsection),
132 during the walking task, the data for each gait parameter $(x, y, z, \phi, d\phi/dt)$ were divided into 5
133 segments (1 minute each one) and the PSD was calculated for each of these 5 segments
134 independently. The segments were then averaged across all the parameters and all the subjects
135 leading to a grand average of the PSD. Frequencies ≤ 3 Hz accounted for > 90% of the total PSD
136 for the kinematics. The same segmentation was applied to each channel of the EEG recorded
137 during rest and walking conditions. The PSD of each segment was averaged across channels and
138 then averaged across subjects leading to a grand average. The grand averages for the kinematics

and the EEG were then smoothed with local regression using weighted linear least squares and a 2nd degree polynomial model as implemented in the Matlab's *loess* function with a span (percentage of the total number of data points) of 10%.

Signal preprocessing. Figure 1 shows our decoding methodology. All the data analysis, decoder design and cross-validation procedures were performed off-line using custom software written in MATLAB (Mathworks Inc., Natick, MA). The most frontal electrodes (FP1, FP2, FPz) were removed off-line from all the subjects, as they are usually contaminated by eye-blinks. Temporal electrodes were also removed, as they are most susceptible to artifacts from facial and cranial muscle activity (Goncharova et al. 2003). Signals from each EEG electrode were decimated by a factor of 5 (to 100 Hz), then filtered with a zero-phase, 3rd order, band-pass Butterworth filter (0.1 – 2 Hz) and normalized by subtracting their mean and dividing by their standard deviation (Bradberry et al. 2010). Kinematic data were filtered with a zero-phase, 3rd order, band-pass Butterworth filter (0.1 – 3 Hz), as this frequency range accounted for 90% of the signal power.

Decoding method. A time-embedded (10 lags, corresponding to 100 ms in the past) linear Wiener filter (Bradberry et al. 2010; Carmena et al. 2003; Fitzsimmons et al. 2009*)* was independently designed, optimized, and cross-validated for each extracted gait parameter. The linear model was given by:

$$y(t) = a + \sum_{n=1}^{N}\sum_{k=0}^{L} b_{nk} S_n(t-k) + \varepsilon(t)$$

where $y(t)$ is the gait parameter measured $(x, y, z, \phi, d\phi/dt)$ time series representing the linear and angular kinematics, and their time derivatives, for the hip, knee and ankle joints; L and N are the number of lags and the number of electrodes, respectively; $S_n(t-k)$ is the standardized voltage measured at EEG electrode n at lag time k, a and b are weights obtained through multiple linear regression and $\varepsilon(t)$ is the residual error. The parameters of the

model were calculated using the standard GLM functions in MATLAB under the Gaussian distribution using the Matlab's linear *link* function.

Model performance metrics. In order to assess and compare the predictive power of each decoder (neural decoders were trained independently for each subject, and each decoded parameter), a 5-fold cross validation procedure; i.e., 5 distinct sets of test data that were not used to train the decoder were employed for testing purposes. That is, the data recorded during the 5 minutes of the walking task were divided into 5 segments (1 minute each one). Four segments were used for training, while the remaining segment was used for testing the model. This procedure was repeated for all the possible combinations. The Pearson correlation coefficient (r) was calculated between the known measured signal and the predicted decoder's output as follows:

$$r(x,\hat{x}) = \frac{\mathrm{cov}(x,\hat{x})}{\sigma_x \sigma_{\hat{x}}}$$

where x is the actual measured parameter, $\hat{x}$ is the prediction of that parameter and σ_x and $\sigma_{\hat{x}}$ are the standard deviations of x and $\hat{x}$ respectively.

The SNR (signal to noise ratio) was calculated according to Fitzsimmons et al. (2009).

$$SNR(x,\hat{x}) = 10\log_{10}\left(\frac{Var(x)}{MSE(\hat{x})}\right)$$

where the variance (Var) of the actual measured parameter (signal x) was calculated by subtracting out the mean of the signal, then squaring and averaging the amplitude. The noise or error ($\hat{x}$) was the difference between the predicted and actual measured signal. The mean squared error (MSE) was calculated by squaring the difference, then averaging to get the mean squared error (MSE), or the power of the noise. The ratio between $Var(x)$ and $MSE(\hat{x})$ was converted into a decibel (dB) scale. A SNR with a value of "0" means that the signal and the noise are equally present in the reconstructed kinematic parameter. A $SNR < 0$ (poor prediction) indicates a noisy reconstruction, while a $SNR > 0$ (good prediction) indicates a high-quality reconstruction of the signal.

194

195 *Sensor dropping analysis.* A sensor dropping analysis (SDA) was used to evaluate the
196 importance of groups of sensors of different sizes to decoding accuracy (e.g., Carmena et al.
197 2003; Fitzsimmons et al. 2009). First, decoder models were trained by using each lag of each
198 sensor (one lag at a time) with the above mentioned 5-fold cross validation procedure. In order to
199 rank the sensors, two different methods were then used based on which kinematic parameter was
200 to be decoded. For the joint angle (ϕ) and the angular velocity $(d\phi/dt)$ the sensors were ranked
201 based on the maximum value of the correlations calculated at each lag. For the Cartesian
202 positions (x, y, z) reconstructions, the sensors were ranked according to the following sensor
203 sensitivity curve equation (Bradberry et al. 2010):

204
205
206
$$R_n = \frac{1}{L+1}\sum_{k=0}^{L}\sqrt{c_{nkx}^2 + c_{nky}^2 + c_{nkz}^2},$$

207 where L is the number of lags, R_n is the rank of sensor n and c are the best correlation
208 coefficients for each Cartesian position (x, y, z). These procedures were followed for all the 45
209 sensors used for decoding after removing the most prefrontal and temporal electrodes. The best
210 34 and 16 sensors out of the 45 sensors ranked were then used for training and testing the
211 decoders for each kinematic parameter extracted.

212

213 *Decoding kinematics by regions of interest (ROI).* In order to assess the contribution to the
214 decoding of each scalp area, the scalp was divided into 5 major ROIs: prefrontal (PF), central
215 (SM), posterior-occipital (PO) and right (RH) and left (LH) hemispheres. The kinematics were
216 decoded using the sensors belonging to each of these ROIs, leading to 5 different decoders for
217 each parameter for each joint and each subject.

218

219 *Scalp Maps*. To visualize the relative contributions of scalp regions to the reconstruction of the
220 position (x, y, z), joint angle (ϕ) and the angular velocity $(d\phi/dt)$ of the hip, knee and ankle
221 joints, the squared correlation (i.e., variance) values c for each sensor at each lag were projected

into a time series of scalp maps (-100-0 ms in increments of 10 ms for a total of 11 scalp maps). The *topoplot* function of EEGLAB [Delorme and Makeig 2004 (http://sccn.ucsd.edu/eeglab/)] was used to plot the correlation values. The contribution of the reconstruction of each lag, for the Cartesian data, was calculated as follows (Bradberry et al. 2010):

$$\%T_i = \%100 * \frac{\sum_{n=1}^{N} \sqrt{c^2_{nix} + c^2_{niy} + c^2_{niz}}}{\sum_{n=1}^{N}\sum_{k=0}^{L} \sqrt{c^2_{nix} + c^2_{niy} + c^2_{niz}}}$$

for all i from 0 to L, where $\%T_i$ is the percentage of reconstruction contribution at time lag i.

Artifacts. To address the issue of potential mechanical artifacts introduced by motion of the EEG cap wires to the recording amplifiers (due in turn to movement of the subject) the phase-locking value (PLV) (Lachaux et al. 2000, 2002) was computed by using Morlet wavelets (Tallon-Baudry et al. 1997). We made the assumption that if the motion of the EEG wires corrupted in some way the measured EEG signals, this problem should have been observed in all the electrodes as the wires were bundled in a single connector. We were particularly interested in investigating the phase in the 1-2 Hz range, as these were the main frequencies used for decoding. We calculated the PLV between each electrode for the walking task and the corresponding kinematics recorded from the subjects. The averaged values of PLV at 1 and 2 Hz were averaged across the electrodes, leading to a mean value at the two frequencies of interest, and compared with the correlation values of the decoding.

Analysis of potential eye movement contributions to decoding. In order to assess a potential contribution of the movement of the eyes to decoding, the decoding process was also carried out by adding the standardized vertical electrooculogram (VEOG) activity to the optimal set of electrodes used for decoding (Bradberry et al. 2011). The r-values and the regression weights were calculated in this new condition. We compared the *r*-values with and without the VEOG electrode by calculating the difference in % and divided the absolute value of the regression weights of the eye-electrode by the sum of the absolute value of all the regression weights of the best fold.

252

253 **Results**

254 *Spectral signature of walking kinematics and associated high-density EEG.* The power spectral
255 density (PSD) of the gait kinematics (black) in the 0.1 – 5 Hz range along with the 95%
256 confidence intervals (gray) are depicted in Figure 2A. The PSD shows that > 90% of the power is
257 contained in the 0.1 – 3 Hz frequency band with a peak (26.45 dB) at ~1.8 Hz. The ratio between
258 upper and lower bounds of the confidence interval throughout all the frequencies was ~6.6 dB.
259 Confidence intervals (95%) of the PSD of the EEG at rest (black) and during precision walking
260 (gray) are shown in Figure 2B. Notably, PSD(walking) > PSD(rest) in the delta and theta bands
261 (~0.1 – 7 Hz) and in the low beta range (13 – 18 Hz), whereas for frequencies > 18 Hz the
262 PSD(walking) < PSD(rest). Importantly, the suppression in the *mu* band observed during upper
263 limb movements (Pfurtscheller et al. 2006) is also present during precision walking in the 8 – 12
264 Hz range. This is clearly depicted in the plot of the ratio of PSD(walking) to PSD(rest) shown in
265 the inset. Of note, the ratio in the 0.1 – 2 Hz range used for decoding was ~ 1.0 dB implying that
266 walking did not alter the spectral signature in this low frequency band (i.e., low delta) – a finding
267 consistent with the data reported by Gwin et al. (2010).

268

269 *Decoding accuracy.* Our EEG decoding method was able to reconstruct 3D linear and angular
270 kinematics of the ankle, knee and hip joints with high accuracy. In order to quantify the level of
271 accuracy, we computed the Pearson's *r* and the *SNR* between measured and predicted Cartesian
272 positions, joint angles and angular velocities across cross-validation folds. *SNR* proved to be a
273 more sensitive measure compared to *r*, which describes the correspondence of signal waveforms,
274 but is insensitive to amplitude scaling and offsets. The average of the correlation values (*r*)
275 between predicted and recorded kinematics for the six subjects was 0.75 (±0.1) and the signal-to-
276 noise ratio values > 0 (4.13 ± 2.03) in all but one measure (subject S6: x axis of the ankle; *SNR* =
277 -0.35±1.09) confirmed the good quality of the decoded signals. Overall, correlation values across
278 the subjects were slightly higher for joint angle (mean $r = 0.78 \pm 0.1$) and angular velocity (mean r
279 $= 0.78 \pm 0.09$) than for Cartesian positions (mean $r_{x,y,z} = 0.71 \pm 0.13$). Figures 3(A) and 3(B), show,

respectively, examples of the measured (black) and the reconstructed (gray) kinematics for the best (S4) and worst (S5) subjects in terms of decoding accuracy. As it can be seen, even in the case of the worst case we were able to decode the kinematic parameters with an accuracy r =0.67 ± 0.09. The quality of the reconstructions of the gait trajectories in 3D space is shown in Figure 4, where an example of the actual and predicted angular velocities and joint angles, and their relative phasing, for the ankle, knee and hip, for subject S4 are depicted in 3D space as well.

Table 1 reports the mean and the standard deviation (SD) of the correlation coefficients (r) and of the *SNR* (dB) values across cross validation folds for all subjects, the best (S4) and worst (S5) cases (subjects), and for intra-cortical recordings from rhesus monkey 1 (Fitzsimmons et al. 2009), while Figure 5 shows the distribution of the correlation coefficients (r) versus *SNR* (dB) for the 6 subjects and for the 2 rhesus monkeys reported in the Fitzimmons' experiment. All the decoded accuracies resulted in mean r values > 0.5 and high *SNR* values (all but one > 0), which were comparable with the values reported using recording spikes from rhesus monkeys (Fitzsimmons et al. 2009). In order to rule out the hypothesis that the visual feedback aided decoding, we report in Table 2 the r and *SNR* values of the best and worst subject decoded under natural walking conditions (no visual feedback and no stripe to step over) from our ancillary task. We used the neural decoders, previously trained using data from the precision walking task, to predict the linear and angular kinematics during normal walking. The decoding accuracies reported for the two conditions were comparable. The averages of the correlation values (r) between predicted and recorded kinematics for the precision and natural walking task for S4 were respectively 0.85±0.08 and 0.7±0.13, while for S5 were respectively 0.67±0.09 and 0.78±0.12.

Decoding accuracy by Region of Interest (ROI). Figure 6 depicts the mean decoding accuracy across the three joints for the 5 different ROIs. For both the angular velocity and the joint angle the r and *SNR* values were higher when all the sensors found during the decoder optimization phase were used to decode. Decoders built based on a subset of electrodes comprising the right (RH) or left (LH) hemispheres scalp regions showed the highest r values among the selected ROIs, while the subset of electrodes spanning the central scalp ROI (SM) showed the lowest r

values. In terms of *SNR*, the right hemisphere, prefrontal; and posterior-occipital ROIs returned the highest values, while the central scalp ROI returned the lowest values. However, statistically these differences were not significant (Kruskal-Wallis test; all comparisons at $p > 0.05$).

Topography of the correlation values of the sensors. The topography of the squared correlation (i.e., variance) values of the sensors at the best lag for the best (subject S4) and worst (subject S5) decoded cases is plotted in Figure 7. These scalp maps represent the individual contribution of electrodes to decoding, that is, the spatial distribution of the EEG information about walking contained at each electrode site. From these scalp maps, it can be inferred that neural information about walking is distributed across a sparse cortical network at the macro-scale of EEG. Scalp maps of sensors most relevant to decoding of the right limb suggest that scalp areas from both hemispheres, somewhat lateralized to the right are involved during walking. Although there are some common scalp regions relevant across all the gait parameters, these scalp regions accounting for the highest variance are different across the two subjects S4 and S5. For instance, C6, FZ, P5, and AF4 electrodes are recruited across gait parameters for subject S4, whereas for subject S5 electrode locations at FC6, P6, and PO2 on the right hemisphere seemed to be relevant for decoding walking across all the kinematic parameters. There were also other important differences across subjects. For example, in subject S4 decoding of both Cartesian and angular kinematics recruited anterior scalp areas (electrode locations AF3, FZ and AF4) that in some cases extended to left frontal sites (F5). These scalp areas were absent in subject S5 who showed the lowest decoding accuracies.

Of note, the scalp maps of the highest (e.g., $r^2 > 0.2$) electrode contributions to decoding the right limb kinematics were rather sparse, particularly for subject S5, who showed rather focal recruitment of electrodes on the right hemisphere, compared with a more bilateral, but still sparse recruitment of electrodes for subject S4. In summary, a sparse network comprised of right posterior-occipital, right lateral, and bilateral anterior-frontal scalp regions appeared to contain decodable gait information.

Minimum number of sensors. Given that the analysis of scalp maps relevant for decoding showed a sparse cortical network for walking, the number of sensors was further optimized using the SDA approach. As shown in Figure 8, the average number of sensors needed to achieve the reported correlations was ~27-32, but on average decoding accuracy reached a phase of plateau (i.e., an improvement in DA $< 5\%$) with 14 sensors (Figure 8A). As shown, with an average of 27 sensors (i.e., the 'best' sensors), the mean r value across the 6 subjects was 0.75 (±0.06) (black bars), while selecting the best 14 sensors led to a mean r value across the 6 subjects of 0.72 (±0.06) (white bars), that is, less than 5% reduction in decoding accuracy (Figure 8B).

Discussion

Gait kinematics can be inferred from scalp EEG signals with high accuracy. This study demonstrates, for the first time, that non-invasive scalp electroencephalographic (EEG) signals can be used to decode kinematic parameters extracted during walking with high accuracy. Of note is the fact that even though we recorded EEG from 60 channels, which some investigators consider to be high-density recordings (Tononi et al. 2010), we showed that as few as 16 sensors were required for decoding with high accuracy. Encouraged by promising results achieved in previous studies carried out in our laboratory (Bradberry et al. 2008, 2009a, 2009b, 2010), we designed neural decoders by using time-domain EEG features extracted solely from the fluctuations in the amplitude (i.e. amplitude modulation or AM) in the EEG signals in the low delta frequency band (0.1 – 2 Hz).

Even though Onton et al. (2005) reported significant changes in the theta band (4 – 8 Hz) reflecting increasing cognitive demands, we emphasize that our decoders were designed to use information contained in the delta band only. Moreover, our decoders were able to predict gait kinematics under two different conditions (precision walking and normal walking), which clearly differ in terms of the cognitive demands and task constraints, and thus changes in cognitive demands or modulations in higher frequency bands could not contribute to decoding.

Our decoding approach proved to be robust as it prevents over-fitting (i.e., by employing separate training and testing trials) and minimize the effect of artifacts because trials with artifacts

364 in the training set would contribute minimally to the learning of the optimal decoder weights, and
365 those in the test set could only reduce, not improve, the decoding accuracy (Tsuchiya et al. 2010).
366 The fact that critical information for decoding lower limb kinematics is contained in the smoothed
367 amplitude modulations (AM) in the lower half of the so-called delta band (i.e., 0.1 – 4 Hz) is
368 consistent with recent EEG, electrocorticographic (ECoG), and local field potential (LFP) upper
369 limb movement decoding studies that use the fluctuations in the amplitude of highly smoothed
370 signals for decoding (Waldert et al. 2008; Lv et al. 2010; Ball et al. 2009; Acharya et al 2010;
371 Ince et al. 2010; and Zhuang et al 2010). It is also consistent with observations by Gwin et al.
372 (2010a), who showed that meaningful changes during walking or running occur at low
373 frequencies (< 10 Hz) in high-density EEG.
374 Fitzsimmons et al. (2009) were the first to prove that linear decoders could be used to
375 reconstruct locomotion, but their experiments were based on intracortical recordings (spikes) in
376 nonhuman primates. Ferris and colleagues have recently shown electrocortical activity coupled to
377 gait cycle phase during treadmill walking in humans (Gwin et al. 2010b), but their study did not
378 decode gait parameters from the EEG signals. In our experiment, 6 subjects were asked to walk at
379 their preferred speed on a treadmill while receiving visual feedback of their lower limbs (through
380 a video monitor at eye level in front of them), to repeatedly avoid stepping on a strip drawn on the
381 treadmill belt – a condition we called *precision walking*. Even though angular kinematics were on
382 average slightly better decoded than linear kinematics, we could not identify any parameter that
383 stood out as the best for decoding, except for the Cartesian "*x*" parameters which showed a lower
384 decoding performance overall. All the kinematic parameters but "*x*" position were decoded with
385 mean *r* values > 0.7 (mean r_x = 0.67 (±0.16), mean r_y = 0.77 (±0.1), r_z = 0.77 (±0.13), r_{angle} = 0.78
386 (±0.09), $r_{ang\ vel}$ = 0.78 (±0.1); and no statistical difference was found among the 5 parameters (p >
387 0.01, ANOVA). Moreover, as shown in Figure 4, the phasing relationship between ankle, knee
388 and hip angular kinematics is preserved in the reconstructed trajectories even though the three
389 joints were decoded independently from each other. Remarkably, as depicted in Figure 6, *SNR*
390 and *r* values were comparable to the ones reported by Fitzsimmons et al. (2009), a result that
391 supports the hypothesis that the EEG signals in the low delta frequency band over a large but

sparse cortical network contain decodable information that could be used to design EEG-based brain-machine interface (BMI) systems for restoration of lower limb movement. It cannot be overemphasized that the same decoders calibrated using data from the precision walking task were able to reconstruct the gait kinematics during normal walking, which did not require subjects to monitor and control foot placement and had not access to visual feedback of foot placement, thus demonstrating the robustness of our methods.

Scalp map analysis. Decoder optimization and scalp maps of correlations for the right limb confirmed that human walking is sub-served by a complex, distributed but sparse cortical network, in which different scalp areas over anterior, right lateral and right anterior-occipital scalp areas seem to equally contribute to the decoding, at least at the macro-scale of EEG. As we decoded the right leg only, it still remains to be seen whether this sparse network that encoded right-side lower limb kinematics would be mirrored in the case of the left leg kinematics.

Our best decoded case (subject S4) showed the highest gait-related information in the bilateral anterior, and the lateral and posterior-occipital scalp areas in the right hemisphere. Of note, our worst subject (subject S5) showed a lack of anterior-frontal recruitment for decoding the right limb, which may explain the lower decoding accuracies. In fact, it is plausible that because the precision walking task presumably involves both visual attention and decision making with respect to deciding when or how best to avoid stepping in the white line drawn on the treadmill, this lack of anterior-frontal recruitment for decoding affected the overall performance. The fact that different scalp brain areas could equally contribute to the decoding is supported by the r and *SNR* values obtained when decoding kinematic parameters using only sensors from specific ROIs. In fact, even though differences in terms of r and *SNR* were observed between the 5 selected ROIs, statistically these differences were not significant. Our observations are in agreement with the findings by Gwin et al. (2010b), who used source analysis and reported electrocortical sources in the anterior cingulate, posterior parietal and sensorimotor cortex associated with intra-stride changes in spectral power. During the end of stance, they also observed that alpha and beta band spectral power increased in or near the left/right sensorimotor and dorsal anterior cingulated

cortex. However, power increases in the left/right sensorimotor cortices were more pronounced for contralateral limb push-off than for ipsilateral limb push-off. Studies carried out using fNIRS also showed involvement of frontal, premotor and supplementary motor areas during walking (Harada et al. 2009; Miyai et al. 2001; Suzuki et al. 2008; Suzuki et al. 2004). These results support the idea that walking is represented across a plurality of cortical brain areas.

Minimum number of sensors. An important issue in brain-machine interface design is concerned with the minimum number of sensors necessary to achieve a reasonable decoding accuracy. As it is well-known (Alpaydin 2004), a common occurrence in machine learning is the fact that as the number of input features increases, the decoding accuracy of the predictions increases up to a certain point, after which the model becomes too complicated, over-fitting might occur and as a consequence of this fact performance decreases. Given this, we decided to compare the *r* values obtained with the number of sensors found in the SDA with the best *r* values obtained by using up to 16 sensors. Our results indicate that ~14 sensors could be sufficient to decode human locomotion using EEG.

Variability of the kinematics and its relation with decoding accuracy. Spectral analysis of the gait kinematics showed that more than 90% of the power was retained in the 0.1 – 3 Hz range, justifying our choice to band pass filter the kinematic data within this frequency range. The 6.6 dB ratio of the upper and lower confidence intervals suggested a significant variability of the kinematic parameters across the 6 subjects. This variability could be due to the fact that each subject chose his/her comfortable pace for the walking task, but also varied his/her gait speed during the task. Consistent with upper limb movement decoding studies (Bradberry et al. 2010), a negative correlation between movement variability and decoding accuracy was found when decoding gait parameters for both angular velocity and joint angle decoding (Figure 9). Specifically, the relationship between the decoding accuracy and gait variability, as measured by the kurtosis (kurtosis = 3 implies normal distribution), for angular velocity and the joint angle was estimated. Low values of the kurtosis (~3) (Figure 9) and high decoding accuracy for both

448 the angular velocity and the joint angle suggest that a normal distribution is responsible for an
449 increase in decoding accuracy.
450
451 *Decoding accuracy was not affected nor corrupted by eye, mechanical or EMG artifacts*. The
452 spectral analysis of the EEG showed interesting results. As in the case of the upper limbs
453 (Pfurtscheller et al. 2006), a desynchronization during the walking task was found in the *mu* band
454 (8 – 12 Hz). As reported by Gwin et al. (2010a), PSD values during walking were generally
455 higher than PSD values during rest (i.e., standing) at low frequencies (0.1 – 7 Hz) and in the
456 middle beta band (13 – 18 Hz). The ratio of PSD(walking) to PSD(rest), albeit small (e.g., ~ 1dB
457 in the 0.1 – 2 Hz), is consistent with those observations. Moreover, Gwin et al. (2010) reported
458 that gait-related artifacts removed from EEG signals were insubstantial when subjects walked at a
459 slow pace (0.8m/s = 2.88 km/h). In our experiments, no subject walked faster than 2.4 km/h, thus
460 reducing further the likelihood of mechanical artifacts. Nevertheless, it could still be argued that
461 EEG signals measured during gross motor tasks like walking are prone to a myriad of
462 physiological, mechanical, and environmental artifacts that would prevent accurate measurement
463 and analysis of cortical dynamics during treadmill walking (Gwin et al. 2010a). However, our
464 proposed method for reconstruction of gait parameters and additional analyses of the potential
465 influence of artifactual components to gait decoding suggest otherwise.
466 First, the decoding accuracies with and without inclusion of the vertical electrooculogram
467 (VEOG) electrode were similar. For all the decoded gait parameters except for the ankle in
468 subject 2 (S2, r_y = 5.1%, r_z = 9.6%), the addition of the VEOG electrode increased negligibly the
469 decoding accuracy by a maximum of 3.1%. The contribution of VEOG in terms of regression
470 weights was also negligible for all decoded gait parameters except for the reconstruction of limb
471 trajectories in the ankle's z-dimension for subject 2 (S2, r_z = 28%). Furthermore, S2 showed the
472 lowest *r*-value for the ankle (r_z = 0.31±0.19), supporting the notion that eyes movements did not
473 contribute to the high *r* and *SNR* values found in this study. Results are reported in Table III. It is
474 also important to point out that in the normal walking condition, subject's gaze was instructed to
475 be maintained straight ahead. This condition is likely to be associated with significant eye

movements due to the compensation of displacements of the head during walking (and neck muscle activity). Indeed, significant eye movements have been reported during standing and walking (Gramann et al., 2010). However, two lines of reasoning argue against the potential contributions of eye movement to decoding: First, the same decoder was used to infer limb kinematics in two conditions (normal walking and precision walking) that differed in the pattern of eye movements (gaze straight ahead vs. monitoring foot placement in a monitor), and second, the correlation analysis showed that eye movements did not assist gait decoding.

Second, Goncharova et al. (2003) has shown that electromyographic (EMG) and ocular artifacts do generally occur mainly at frequencies higher than 8 Hz, which is 4 times higher than our frequency cutoff of 2 Hz used for reconstruction. Moreover, Goncharova et al. (2003) reported that EMG activity was localized to the frontal and temporal electrodes in the specific frequency band we used for decoding (delta, < 4 Hz). Therefore, in our study frontal and temporal electrodes were removed from the analysis.

Third, correlation values were also calculated between baseline EEG signals band-pass filtered at 0.1 – 2 Hz and gait kinematics (< 3 Hz) and compared with EEG signals acquired during walking, which we hypothesized contained relevant information about gait parameters. Indeed, our results showed that attempting to map baseline EEG signals to gait parameters resulted in extremely low decoding: as a representative example, the *r* and *SNR* values for the ankle joint angle for our best decoded subject (S4) were 0.05 ± 0.07 and -15.27 ± 33.27, respectively, for the baseline EEG signals, whereas decoding accuracies were high (0.87 ± 0.01 and 6.1 ± 0.59 for *r* and *SNR*, respectively) when using EEG signals acquired during the walking task, confirming that EEG signals measured during walking contained detailed cortical information about gait parameters.

Fourth, to rule out the presence of mechanical artifacts introduced by motion of the EEG cables or walking itself, we computed the phase-locking value (PLV) among sensors. The rationale was that potential motion artifacts due to EEG wires or the subject's motion would affect all sensors equally. To assess the phase-locking value using wavelet analysis, the significance threshold value was set based on the values calculated by Lachaux et al. (2002). In

504 our case, since we used 6 cycles (n_{co}) for the wavelets and 10 cycles (n_{cy}) for the integration
505 window, the significance threshold was estimated to be 0.71. We applied such analysis to both the
506 baseline EEG and the walking EEG conditions. Our results suggest that mechanical artifacts did
507 not play a role in decoding. As a representative example, the mean PLVs across electrodes of our
508 best subject (S4) for the ankle joint angle kinematic during walking were 0.55 ± 0.08 at 1 Hz,
509 0.53 ± 0.05 at 2 Hz and 0.54 ± 0.06 average across 1-2 Hz (the lower bounds for gait-cycles were
510 ≥ 1Hz). Remarkably, when the baseline EEG condition was used, the mean values across
511 electrodes were 0.37 ± 0.02 (at 1 Hz), 0.49 ± 0.03 (at 2 Hz) and 0.43 ± 0.01 (mean of 1 and 2 Hz),
512 which were comparable to those during walking and suggesting lack of mechanical coupling due
513 to concerted wire movement.

514 Fifth, we note that our decoding accuracies were high independently of whether the
515 reconstructed parameters were linear or angular gait kinematics. It is very unlikely that a (global)
516 motion artifact would affect or influence equally both types of gait parameters. For example,
517 mechanical artifacts due to up-down motion would be expected to affect the decoding of vertical
518 trajectories of the hip, ankle and knee joints, but not the decoding of angular joint velocities as
519 they are not linearly related. Nevertheless, the motion of the center of mass (COM), which would
520 be expected to be directly related to that of any upward/downward movement of the EEG wires
521 due to the subject's mechanical motion was very small (sacrum's vertical movement, in meters:
522 S1 = -0.01 ± 0.015, S2 = 0.0006 ± 0.007, S3 = -0.006 ± 0.015, S4 = -0.005 ± 0.013, S5 = -0.0095
523 ± 0.016, S6 = -0.007 ± 0.012). In addition to this, decoding of angular velocities (not linearly
524 related with the 3D translational movements of the cables or the sacrum) for the ankle, hip, and
525 knee resulted in high decoding accuracies that were comparable to the ones of the joint angle and
526 Cartesian positions. Furthermore, it is unlikely that the motion artifact would have been the same
527 for both walking conditions; indeed, the fact that the same decoders were used to decode gait in
528 both walking (precision & normal) conditions is a strong argument against the potential influence
529 of movement artifacts to decoding.

530 Finally, we note that the mapping of the spatial distribution of the highest contributing
531 electrodes to decoding resulted in a sparse but distributed network lateralized to the right

hemisphere with a bilateral anterior contribution suggesting specificity of the cortical representation of the right limb's role in walking is contained in the EEG signal. Our scalp maps allowed us to map electrode locations on the scalp surface according to the maximal amount of information that they might carry about each gait parameter. Remarkably, the scalp maps were different across gait parameters; that is, the amount and type of information about gait was different across electrode sites. As noted above, the same network was used for decoding both walking conditions.

Overall, these results demonstrate the feasibility of employing a noninvasive EEG-based brain-machine interface (BMI) for the restoration of gait. This view is supported by fMRI studies in which cortical activation was detected when subjects imagined themselves walking (Bakker et al. 2007, 2008; Iseki et al. 2008) and when paraplegic patients imagined foot and leg movements (Alkadhi et al. 2005; Cramer et al. 2005; Hotz-Boendermaker et al. 2008). A cortically EEG-driven BMI for the restoration or rehabilitation of walking could be also used as a strategy to harness or potentiate the remaining functionality and plasticity of spinal cord circuits isolated from the brain (Behrman et al. 2006; Grasso et al. 2004; Lunenburger et al. 2006), and as a new tool for assessing the cortical contributions to walking in health and disease, or to study the changes in these contributions during learning and adaptation.

Conclusion. We have shown the feasibility of decoding human walking under precision (attentive, requiring visually-guided foot placement) and normal (subjects's gaze was straight ahead) conditions by using scalp EEG with as few as 16 electrodes. The fact that these two conditions were decoded using the same decoder calibrated in the more complex precision walking task attests to the robustness of the decoding approach. Future studies should investigate the applicability of the present findings to the development of brain-machine interfaces and the suitability of the proposed approach to examine cortical plasticity during gait rehabilitation.

Acknowledgements: This research has been supported by the University of Maryland College Park-University of Maryland-Baltimore Seed Grant Program to JLCV and LF. Support by the VA Maryland Exercise & Robotics Center of Excellence (VA RR&D B3688R) and by the University of Maryland's Department of Kinesiology Graduate Student Research Initiative Fund are gladly acknowledged. We thank Dr. Richard F. Macko for his support and valuable discussions during the performance of this study.

588

589 Figure Captions

590

591 Figure 1: Diagram depicting the decoding methodology. The subject was fitted with a 60 channel
592 EEG cap to record brain activity and a plurality of sensors were used to record 3D kinematics and
593 footswitch data. EEG and kinematics were synchronized, preprocessed and saved. The training,
594 testing and optimization of individual neural decoders, for each decoded gait parameter, were
595 performed off-line using cross-validation procedures.

596

597 Figure 2: A. Mean power spectral density (PSD in dB/Hz, in black) and 95% confidence
598 intervals (in gray) of the grand mean of the kinematic parameters across the six subjects. B.
599 Confidence intervals (95%) of the power spectral density (PSD in dB/Hz) of the EEG recorded
600 during rest and walking of the grand mean (not shown) across the six subjects. The black lines
601 represent the PSD at rest, while the gray lines represent the PSD during walking. The inset shows
602 the ratio PSD (walking) to PSD (rest).

603

604 Figure 3: Reconstructed right leg kinematics from EEG for the 'best' (S4, A) and 'worst' (S5, B)
605 decoded subjects. Columns represent ankle, knee and hip joints. Each row represents comparison
606 of reconstructed (gray) and actual (black) measured linear kinematic trajectories for (x, y, z), joint
607 angle and angular velocity time series at the optimal number of sensors.

608

609 Figure 4: Actual and predicted standardized 3D trajectories for angular velocity and joint angle of
610 the ankle for subject S4. Ankle, knee and hip trajectories are plotted respectively in the x, y and z-
611 axes. The letter "S" represent the starting point. A: trajectories of the predicted (black) vs. actual
612 (gray) angular velocities; B: trajectories of the predicted (black) vs. actual (gray) joint angles.

613

Figure 5: Comparison of decoding accuracy (*r*) vs. *SNR* (dB) for the current study (N=6) with the nonhuman primate study (monkeys 1 and 2) of Fitzsimons et al. (2009). Stars represent monkeys, while squares represent the 6 subjects of our study.

Figure 6: Decoding accuracy from different scalp regions of interest (ROIs). The box plots show the *r* and the *SNR* values for the angular velocity and the joint angle calculated with electrodes situated across 5 different scalp areas: left hemisphere (LH), right hemisphere (RH), anterior (PF), centro-medial (SM), anterior-occipital (PO), and with all the electrodes (ALL). Both *r*-values and the *SNR* values are shown. The scalp map depicts the coverage used for each ROI and the location of the electrodes in each ROI. Right and left hemispheres have been separated by the mid line. Mid-line electrodes (along the line linking FZ and OZ) have been included in neither the right nor the left hemisphere ROIs.

Figure 7: Spatial distribution of r^2 decoding accuracies across sensors for the 'best' (S4) and 'worst' (S5) decoded subjects. Scalp maps represent the spatial distribution of r^2 across electrodes at the best lag for each parameter resulting from the training of the linear model. From left to right, each column represents the scalp map of the Cartesian positions, joint angles and angular velocities.

Figure 8: Decoding accuracy with the optimal number of sensors and the lowest number of sensors. A) Mean (±std) Sensors Dropping Analysis (SDA) across the six subjects. B) Decoding accuracy (*r)* obtained by using the best 34 sensors found by the SDA analysis (black) and by using the highest *r* among the first best 16 sensors (white) for each subject. Each set of 2 bars (black and white) represents the mean *r*-values (±std) for each subject. The last set of two bars represents the grand average across the subjects for both the optimal condition (black) and the plateau condition (white). C) Number of sensors used to compute the *r*-values when the 'best' number of sensors was used (black) and up to 16 sensors were used (white) for each subject. Each set of 2 bars (black and white) represents the *r* values (±std) of the six subjects.

642

643 Figure 9: Relationship between gait variability and decoding accuracy for the angular velocity
644 and joint position trajectories. A) Mean (±std) of the kurtosis of the angular velocity across the
645 three joints (ankle, knee and hip); B) Mean (±std) of the kurtosis of the joint angle across the
646 three joints (ankle, knee and hip); C) Box plots of the confidence intervals (70%) for the
647 bootstrapped *r, kurtosis paired* values. The horizontal line represents the medians.

648

649

650

651

652 **References**
653

654 **Acharya S, Fifer MS, Benz HL, Crone NE, Thakor N.** Electrocorticographic amplitude
655 predicts finger positions during slow grasping motions of the hand *J Neural Eng* 7 046002
656 doi: 10.1088/1741-2560/7/4/046002, 2010
657

658 **Alkadhi H, Brugger P, Boendermarker SH, Crelier G, Curt A, Hepp-Reymond MC, Kollias**
659 **SS.** What disconnection tells about motor imagery: evidence from paraplegic patients *Cereb*
660 *Cortex* 15: 131-140, 2005
661

662 **Alpaydin E.** Introduction to machine learning. *Cambridge*, MA:MIT, 2004, p. 254
663

664 **Ball T, Schulze-Bonhage A, Aertsen A, Mehring C.** Differential representation of arm
665 movement direction in relation to cortical anatomy and function *J Neural Eng* 6: 016006, 2009
666

667 **Bakker M, de Lange FP, Stevens JA, Toni I Bloem BR.** Motor imagery of gait: a quantitative
668 approach *Exp Brain Res* 179: 497-504, 2007
669

670 **Bakker M, de Lange FP, Helmich RC, Scheeringa R, Bloem BR, Toni I.** (2008) Cerebral
671 correlates of motor imagery of normal and precision gait *Neuroimage* 41: 998-1010, 2008
672

673 **Behrman AL, Bowden MG, Nair PM.** Neuroplasticity after spinal cord injury and training: an
674 emerging paradigm shift in rehabilitation and walking recovery *Phys Ther* 86: 1406-1425, 2006
675

676 **Bradberry TJ, Contreras-Vidal JL, Rong F.** Decoding hand and cursor kinematics from
677 magnetoencephalographic signals during tool use *Conf Proc IEEE Eng Med Biol Soc*; 5306:5309,
678 2008
679

Bradberry TJ, Rong F and Contreras-Vidal JL. Decoding center-out hand velocity from MEG signals during visuomotor adaptation *Neuroimage* 47: 1691:1700, 2009a

Bradberry TJ, Gentili R, Contreras-Vidal JL. Decoding three dimensional hand kinematics from electroencephalographic signals *Conf Proc IEEE Eng Med Biol Soc*; 5010:5013, 2009b

Bradberry TJ, Gentili RJ, Contreras-Vidal JL. Reconstructing Three-Dimensional Hand Movements from Noninvasive Electroencephalographic Signals *J Neurosci* 30: 3432-3437, 2010

Bradberry TJ, Gentili RJ, Contreras-Vidal JL. Fast attainment of computer cursor control with noninvasively acquired brain signals *J Neural Eng* 8(3):036010

Carmena JM, Lebedev MA, Crist RE, O'Doherty JE, Santucci DM, Dimitrov DF, Patil PG, Henriquez CS, Nicolelis MA. Learning to control a brain-machine interface for reaching and grasping by primates *PLoS Biol.* 1, E42, 2003

Choi JT, Bastian AJ. Adaptation reveals independent control networks for human walking *Nature Neuroscience* 10: 1055 – 1062, 2007

Christensen LO, Andersen JB, Sinkjær T, Nielsen J. (2001) Transcranial magnetic stimulation and stretch reflexes in the tibialis anterior muscle during human walking *The Journal of Physiology*, 531: 545-557, 2001

Cramer SC, Lastra L, Lacourse MG, Cohen MJ. Brain motor system function after chronic, complete spinal cord injury *Brain* 128: 2941-2950, 2005

Delorme A, Makeig S. EEGLAB: an open source toolbox for analysis of single-trial EEG dynamics including independent component analysis *J Neurosci Methods* 134: 9-21, 2004

709 **Dobkin BH, Firestine A, West M, Saremi K and Woods R.** Ankle dorsiflexion as an fMRI
710 paradigm to assay motor control for walking during rehabilitation *Neuroimage* 32: 370-381, 2004
711
712 **Fitzsimmons NA, Lebedev MA, Peikon ID, Nicolesis MA.** Extracting kinematic parameters for
713 monkey bipedal walking from cortical neuronal ensemble activity *Front. Integr Neurosci.* 3:3.
714 doi:10.3389/neuro.07.003.2009, 2009
715
716 **Goncharova II, McFarland DJ, Vaughan JR, Wolpaw JR.** EMG contamination of EEG:
717 spectral and topographical characteristics *Clin Neurophysiol* 114: 1580-1593, 2003
718
719 **Gramann K, Gwin JT, Bigdely-Shamlo N, Ferris DP, Makeig S.** Visual evoked responses
720 during standing and walking *Frontiers in Human Neuroscience*, 4:202, 2010
721
722 **Grasso R, Ivanenko YP, Zago M, Molinari M, Scivoletto G, Castellano V, Macellari V,**
723 **Lacquaniti F.** Distributed plasticity of locomotor pattern generators in spinal cord injured
724 patients *Brain* 127: 1019-1034, 2004
725
726 **Grillner S, Wallén P, Saitoh K, Kozlov A, Robertson B.** Neural Bases of goal-directed
727 locomotion in vertebrates – An overview *Brain Research Reviews* 57: 2-12, 2008
728
729 **Gwin JT, Grasman K, Makeig S, Ferris DP.** Removal of movement artifact from high-density
730 EEG recorded during walking and running *J Neurophysiol* 103: 3526-3534, 2010a
731
732 **Gwin JT, Grasman K, Makeig S, Ferris DP.** Electrocortical activity is coupled to gait cycle
733 phase during treadmill walking *J Neuroimage* 54(2): 1289-96, 2010b
734
735 **Harada T, Miyai I. ,Kubota K.** Gait capacity affects cortical activation patterns related to speed
736 control in the elderly *Exp Brain Res* 193: 445-454, 2009

737

738 **Heuninckx S, Wenderoth N, Debaere F, Peeters R, Swinnen SP.** Neural Basis of Aging: The
739 Penetration of Cognition into Action Control *J of Neurosci*, 25(29): 6787-6796, 2005
740 **Heuninckx S, Wenderoth N, Swinnen SP.** Systems Neuroplasticity in the Aging Brain:
741 Recruiting Additional Neural Resources for Successful Motor Performance in Elderly Persons *J*
742 *of Neurosci*, 28(1): 91-99, 2008
743
744 **Iseki K, Hanakawa T, Shinozaki J, Nankaku M, Fukuyama H.** Neural mechanisms involved
745 in mental imagery and observation of gait *Neuroimage* 41: 1021-1031, 2008
746
747 **Jerbi K, Lachaux J P, N'Diaye K, Pantazis D, Leahy R M, Garnero L, Baillet S.** Coherent
748 neural representation of hand speed in humans revealed by MEG imaging *Proc Natl Acad Sci*
749 USA 104: 7676-7681, 2007
750
751 **Lachaux JP, Rodriguez E, Le Van Quyen M, Lutz A, Martinerie J, Varela FJ.** Studying
752 single-trials of phase synchronous activity in the brain *J Bifurcation and Chaos* 10(10): 2429-
753 2439, 2000
754
755 **Lachaux JP, Lutz A, Rudrauf D, Cosmelli D, Le Van Quyen M, Martinerie J, Varela FJ.**
756 Estimating the time-course of coherence between single-trial brain signals: an introduction to
757 wavelet coherence *Clin Neurophysiol* 32: 157-174, 2002
758
759 **Luft A, Smith GV, Forrester L, Whitall G, Macko RF, Hauser TK, Goldberg AP, Hanley**
760 **DF** Comparing brain activation associated with isolated upper and lower limb movement across
761 corresponding joints *Human Brain Mapping* 17: 131-140, 2002
762
763 **Lunenburger L, Bolliger M, Czell D, Muller R, Dietz V.** Modulation of locomotor activity in
764 complete spinal cord injury *Exp Brain Res* 174: 638-646, 2006

765

766 **Lv J, Yuanqing L, Zhenghui G.** Decoding hand movement velocity from electroencephalogram
767 signals during a drawing task *Biomedical Engineering Online* 9: 64 doi:10.1186/1475-925X-9-64,
768 2010

769

770 **Miyai I, Tanabe HC, Sase I, Eda H, Oda I, Konishi I, Tsunazawa Y, Suzuki T, Yanagida T,**
771 **Kubota K.** Cortical mapping of gait in humans: a near-infrared spectroscopy topography study
772 *Neuroimage* 14: 1186-1192, 2001

773

774 **Nielsen JB.** How we walk: central control of muscle activity during human walking
775 *Neuroscientist* 9: 195–204, 2003

776

777 **Onton J, Delorme A, Makeig S.** Frontal midline EEG dynamics during working memory
778 *NeuroImage* 27: 341-356, 2005

779

780 **Pfurtscheller G, Brunner C, Schlögl, Lopes da Silva FH.** Mu rhythm (de)synchronization and
781 EEG single-trial classification of different motor imagery tasks *NeuroImage* 31: 153-159, 2006

782

783 **Rossignol S, Schwab M, Schwartz AB, Fehlings MG.** Spinal cord injury: time to move? *J.*
784 *Neurosc.* 27: 11782-11792, 2007

785

786 **Sahyoun C, Floyer-Lea A, Johansen-Berg H, Matthews PM.** Towards an understanding of
787 gait control: brain activation during the anticipation, preparation and execution of foot
788 movements *Neuroimage* 21: 568-575, 2004

789

790 **Suzuki M, Miyai I, Ono T, Oda I, Konishi I, Kochiyama T, Kubota K.** Prefrontal and
791 premotor cortex are involved in adapting walking and running speed on the treadmill: an optical
792 imaging study *Neuroimage* 23: 1020-1026, 2004

Suzuki M, Miyai I, Ono T, Kubota K. Activities in the frontal cortex and gait performance are modulated by preparation. An fNIRS study *Neuroimage* 39: 600-607, 2008

Tallon-Baudry C, Bertrand O, Delpuech C, Pernier J. Oscillatory γ-Band (30-70 Hz) activity induced by a visual search task in humans. *J. Neurosci* 17(2): 722-734, 1997

Tononi G, Riedner BA, Hulse BK, Ferrarelli F, Sarasso S. Enhancing sleep slow waves with natural stimuli. *Medicamundi* 54(2): 82-88, 2010

Tsuchiya N, Kawasaki H, Oya H, Howard MA 3rd, Adolphs R. Decoding face information in time, frequency and space from direct intracranial recordings of the human brain *PloS One* 3(12): e3892 doi: 10.1371/journal.pone.0003892, 2008

Van den Broek SP, Reinders F, Donderwinkel M, Peters MJ. Volume conduction effects in EEG and MEG Electroenceph. *Clin Neurophysio*l 64: 159-170, 1998

Waldert S, Preissl H, Demandt E, Braun C, Birbaumer N, Aertsen E, Mehring C. Hand movement direction decoded from MEG and EEG *J Neurosci* 28: 1000-1008, 2008

Wieser M, Haefeli J, Butler L, Jancke L, Riener R, Koeneke S. Temporal and spatial patterns of cortical activation during assisted lower limb movement *Exp Brain Res* 203: 181-191, 2010

Zhuang J, Truccolo W, Vargas-Irwin C, Donoghue JP. Decoding 3-D reach and grasp kinematics from high-frequency local field potentials in primate primary motor cortex. *IEEE Trans Biomed Eng* 57(7):1774-84, 2010

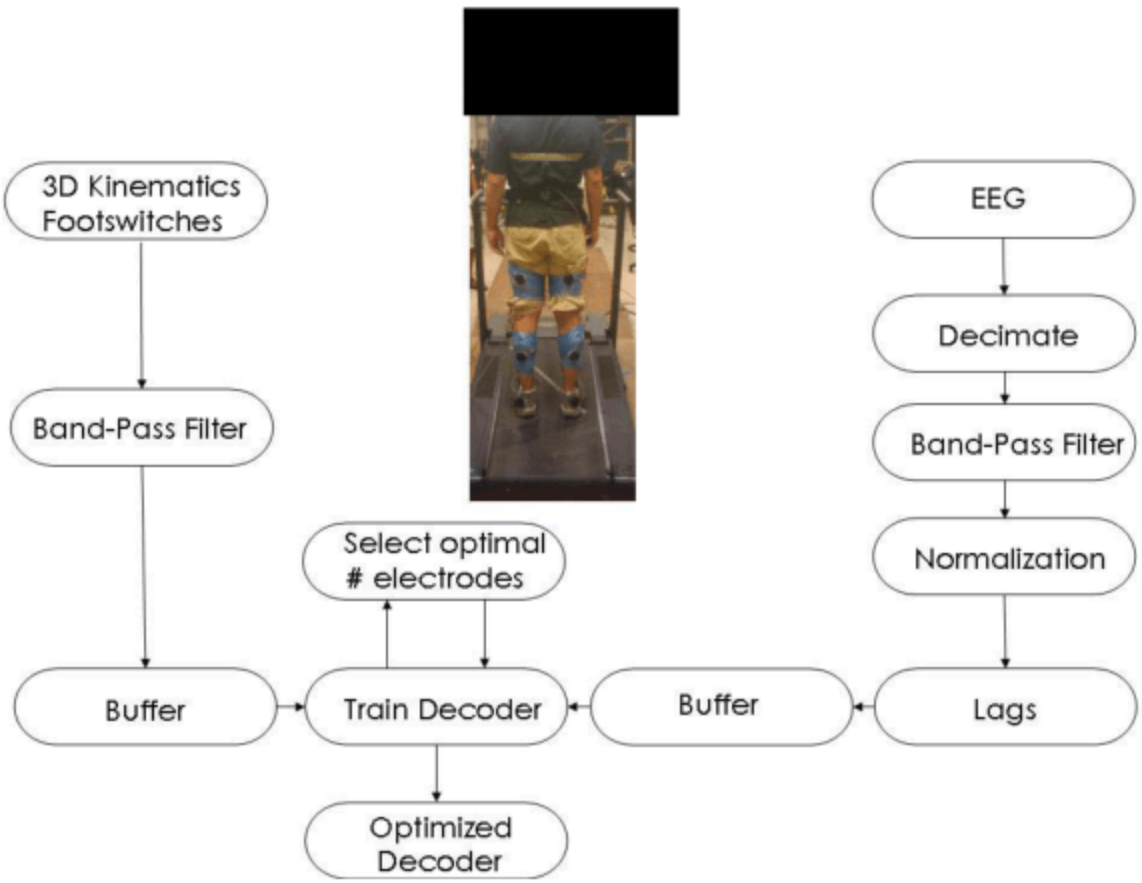
3D Kinematics
Footswitches
Band-Pass Filter
Buffer
Select optimal
electrodes
Train Decoder
Optimized
Decoder
Buffer
Lags
EEG
Decimate
Band-Pass Filter
Normalization

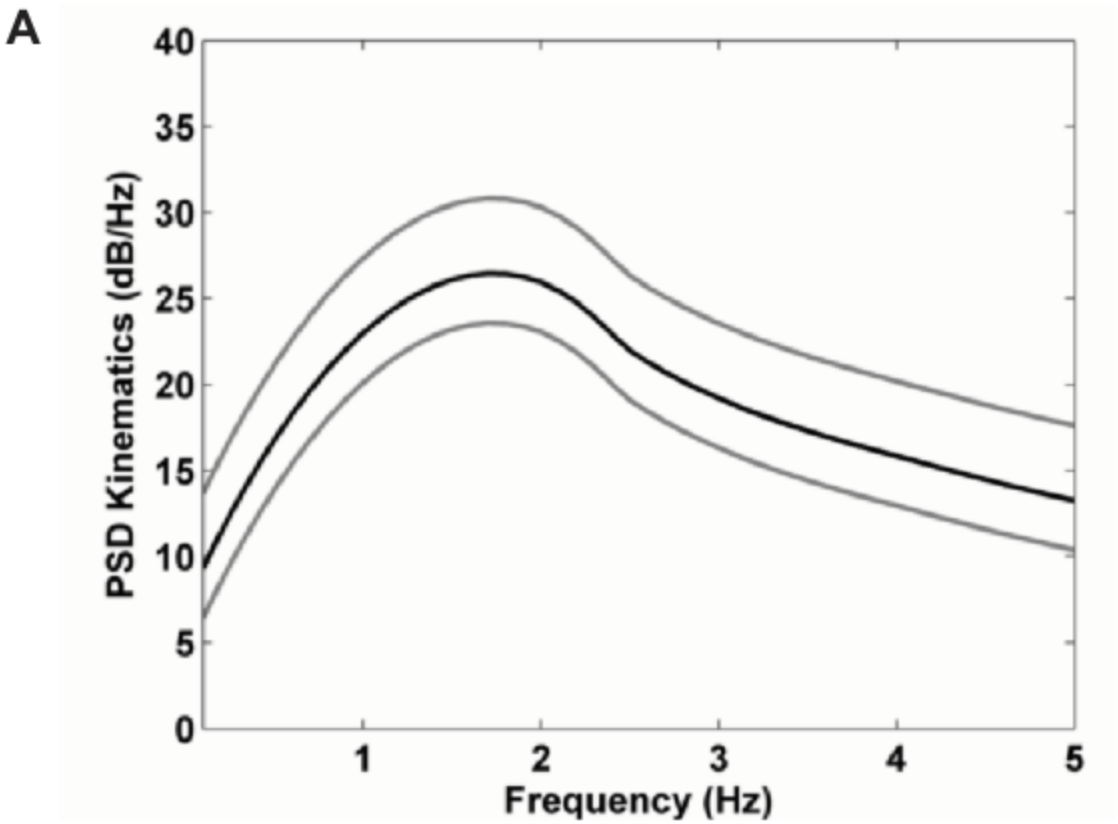
A
PSD Kinematics (dB/Hz)
Frequency (Hz)
0
5
10
15
20
25
30
35
40
1
2
3
4
5

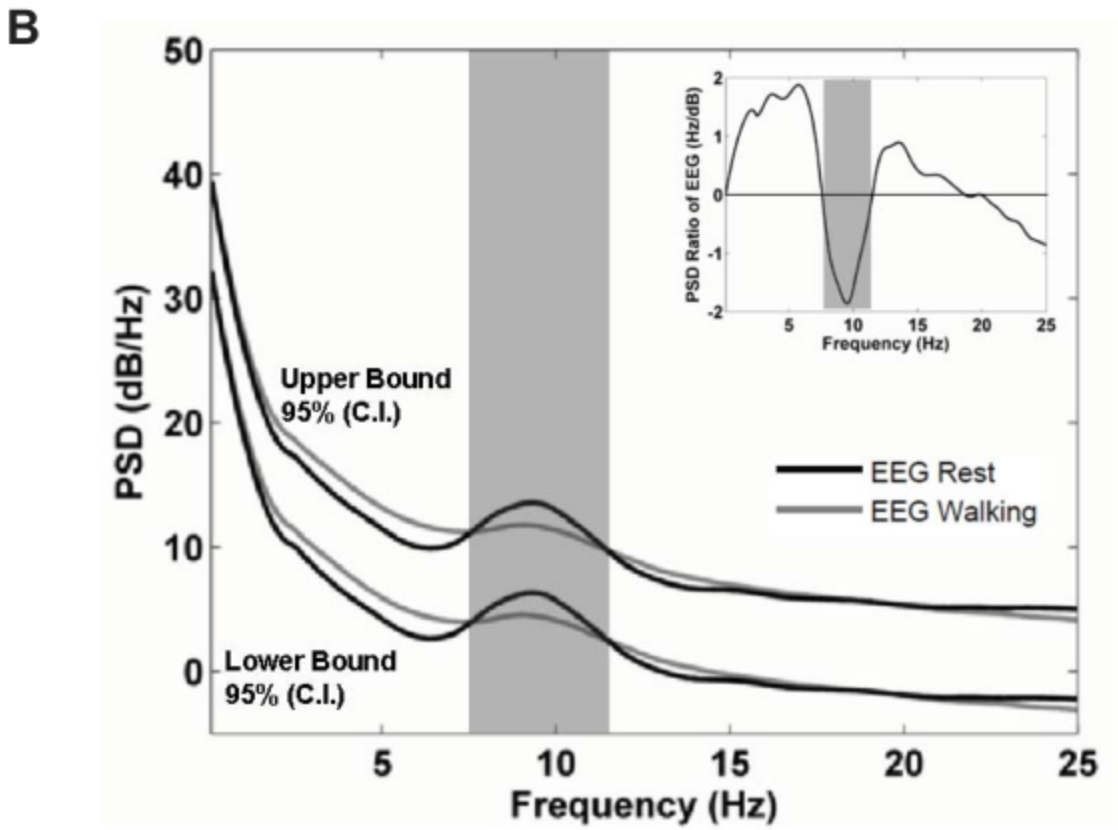
B
PSD (dB/Hz)
Frequency (Hz)
Upper Bound
95% (C.I.)
Lower Bound
95% (C.I.)
EEG Rest
EEG Walking
PSD Ratio of EEG (Hz/dB)
Frequency (Hz)

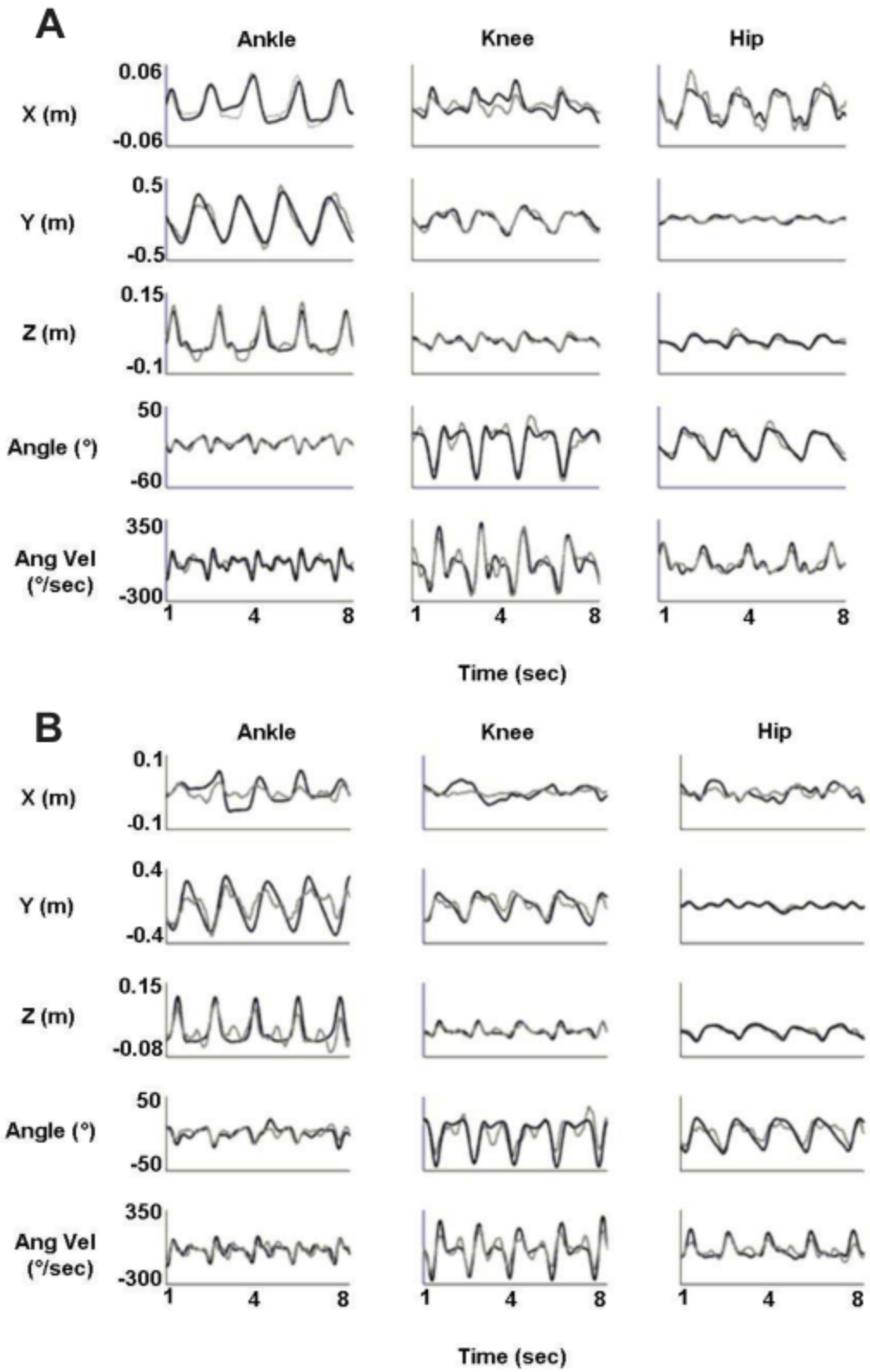

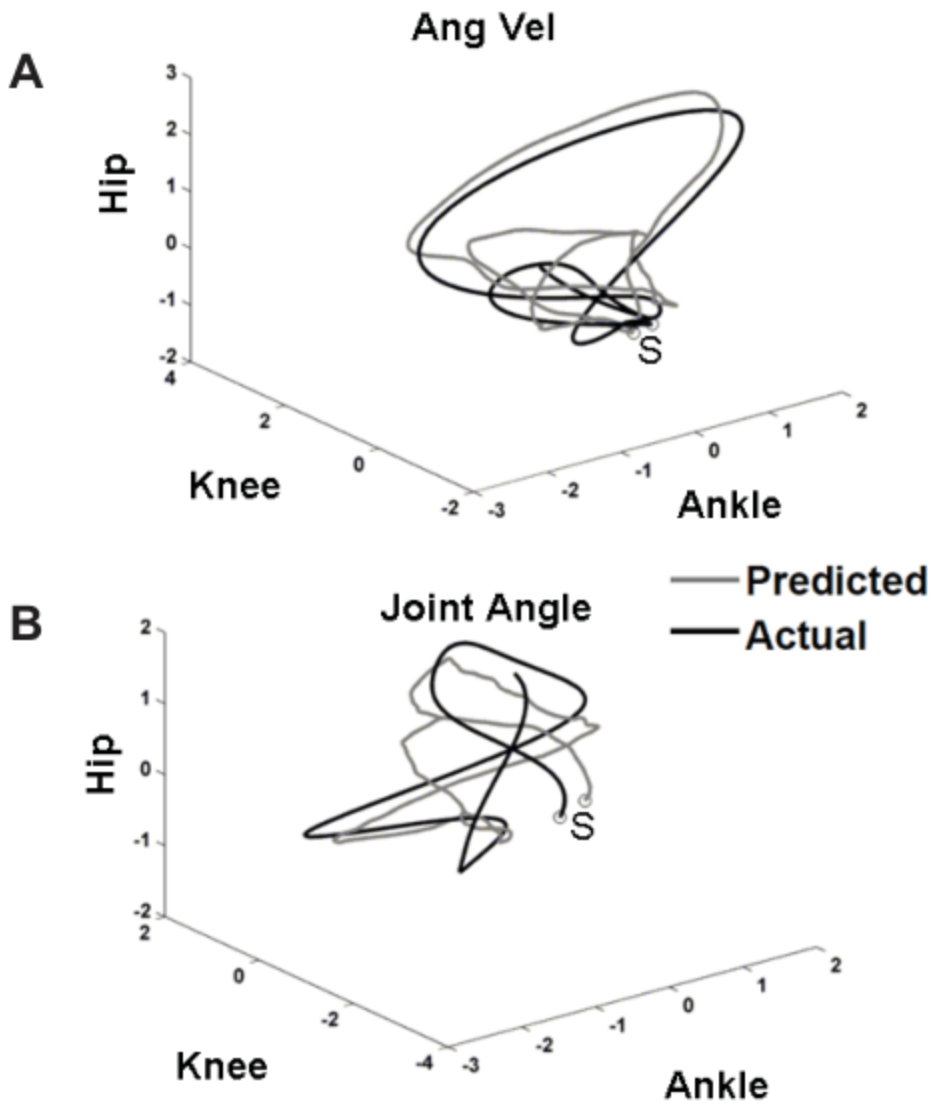
A
Ang Vel
Hip
Knee
Ankle
S
B
Joint Angle
Hip
Knee
Ankle
S
Predicted
Actual

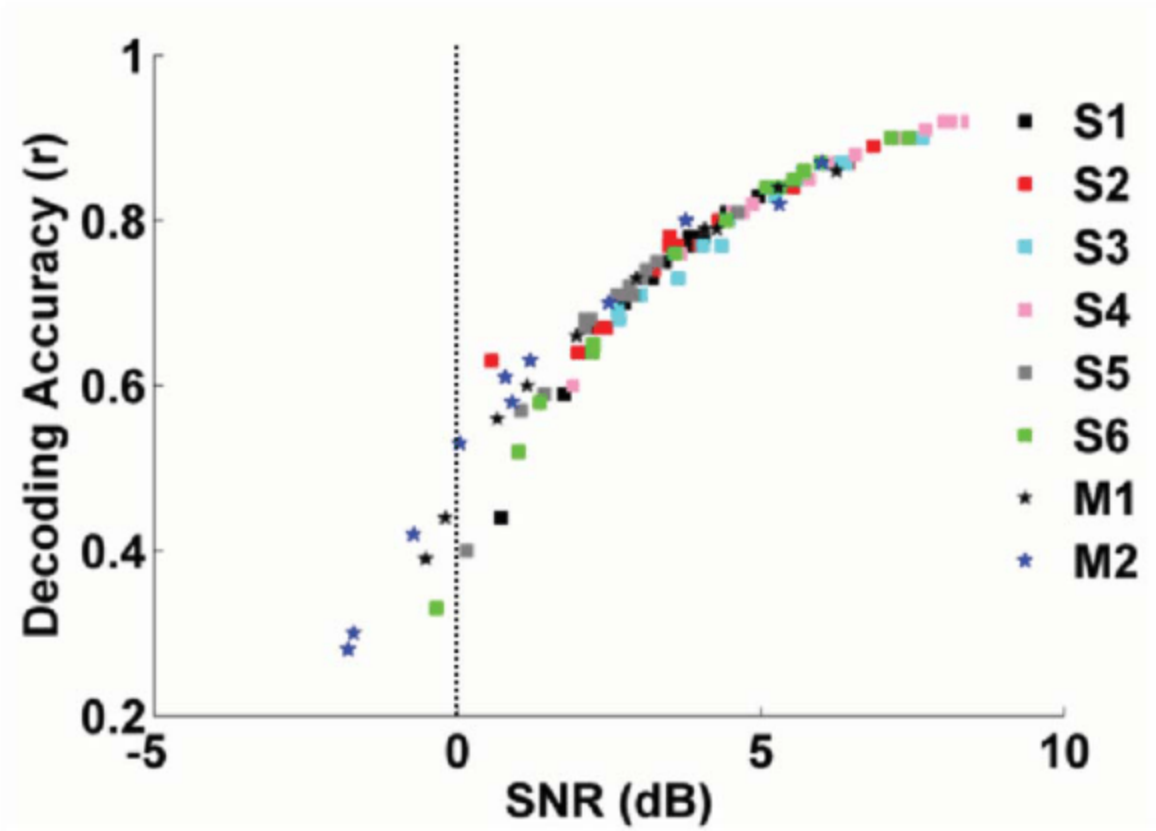
Decoding Accuracy (r)
1
0.8
0.6
0.4
0.2
-5
0
5
10
SNR (dB)
S1
S2
S3
S4
S5
S6
M1
M2

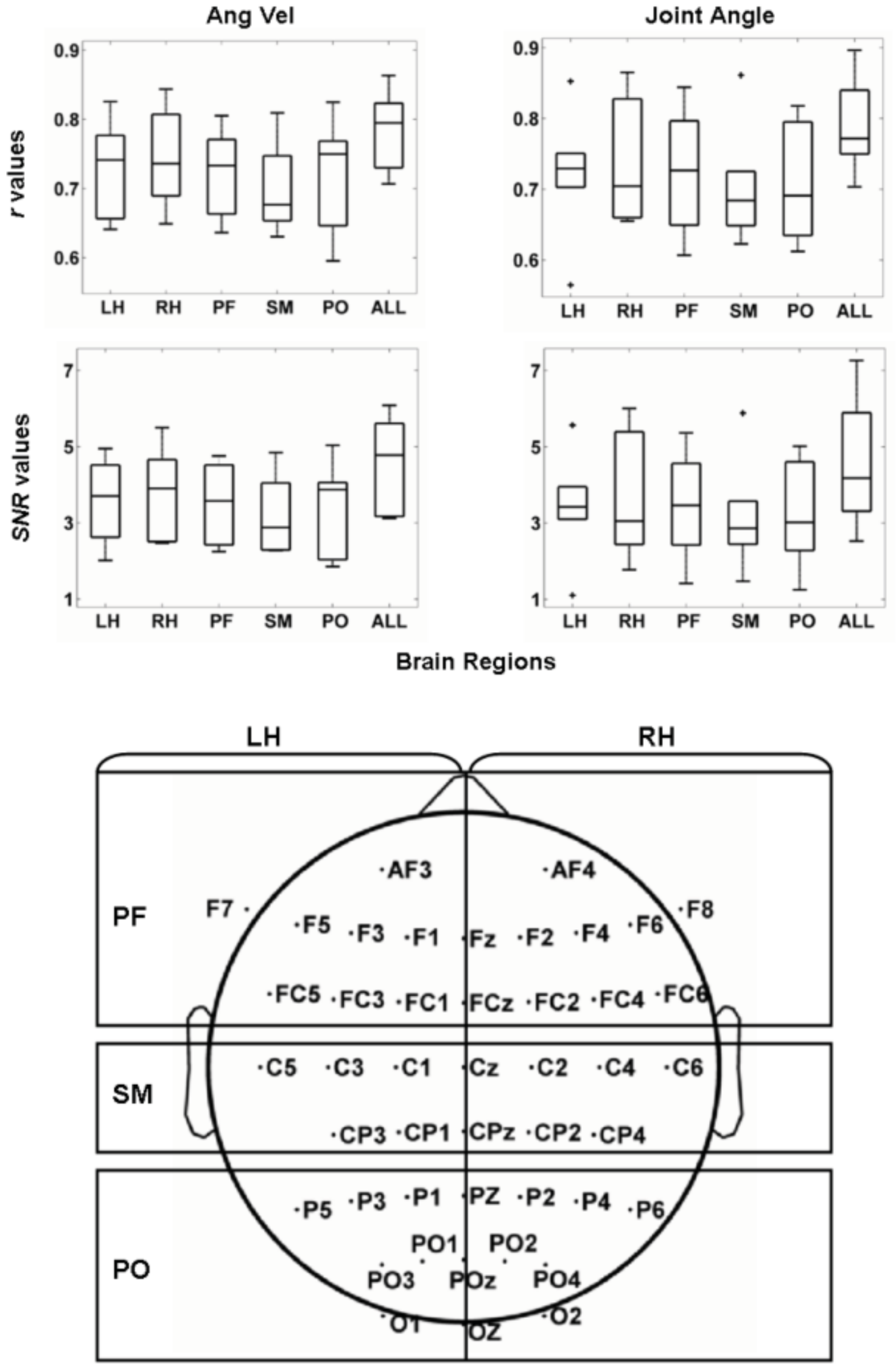
Ang Vel
Joint Angle
r values
SNR values
0.9
0.8
0.7
0.6
7
5
3
1
LH
RH
PF
SM
PO
ALL
Brain Regions
LH
RH
PF
SM
PO
AF3
AF4
F7
F8
F5
F3
F1
Fz
F2
F4
F6
FC5
FC3
FC1
FCz
FC2
FC4
FC6
C5
C3
C1
Cz
C2
C4
C6
CP3
CP1
CPz
CP2
CP4
P5
P3
P1
PZ
P2
P4
P6
PO1
PO2
PO3
POz
PO4
O1
OZ
O2

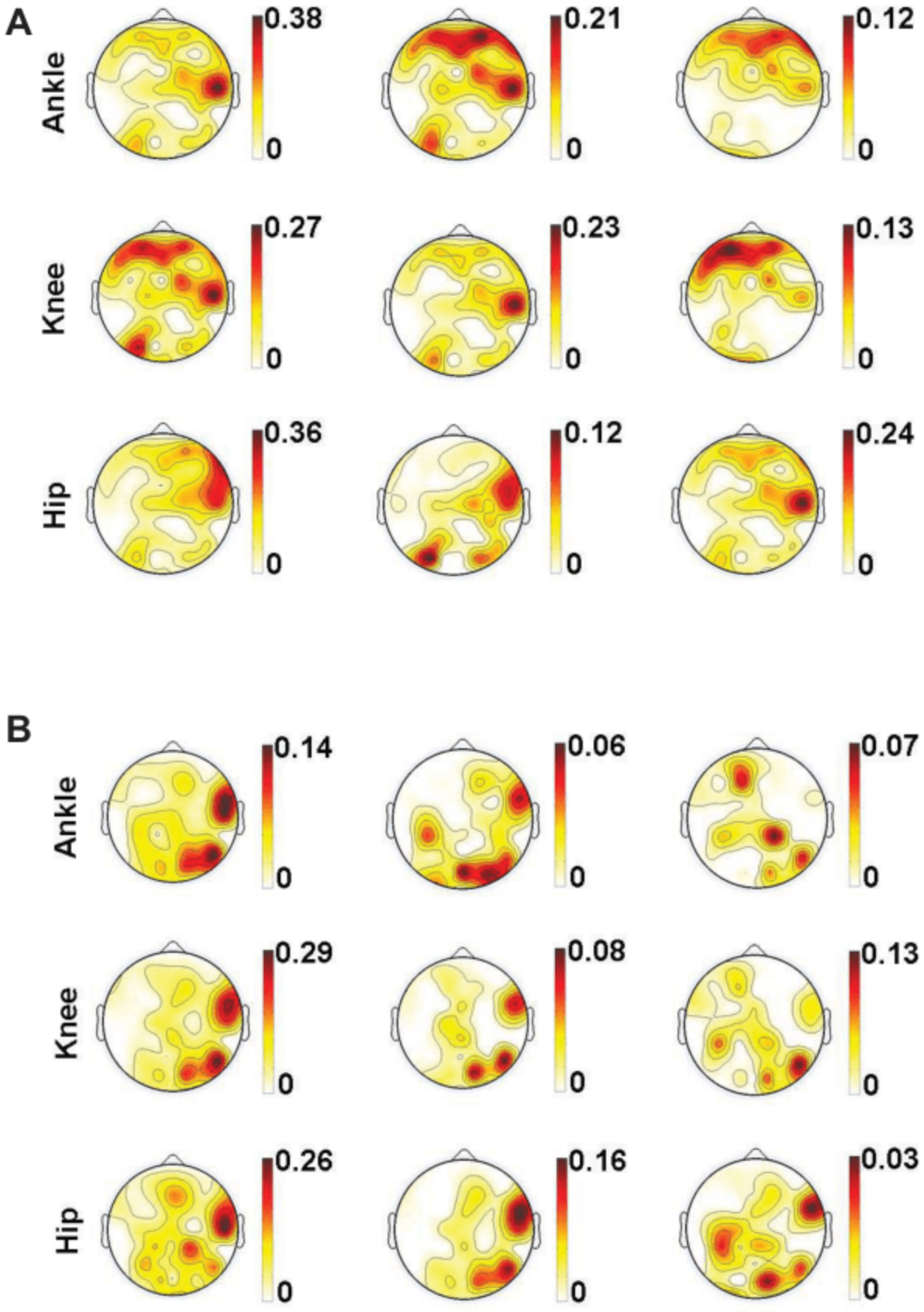
A
Ankle
0.38
0
0.21
0
0.12
0
Knee
0.27
0
0.23
0
0.13
0
Hip
0.36
0
0.12
0
0.24
0
B
Ankle
0.14
0
0.06
0
0.07
0
Knee
0.29
0
0.08
0
0.13
0
Hip
0.26
0
0.16
0
0.03
0

A

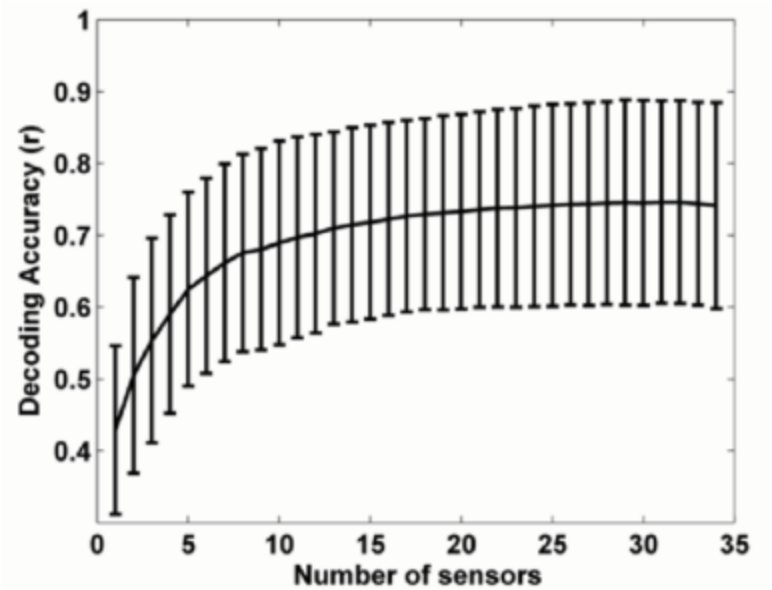
Decoding Accuracy (r)
1
0.9
0.8
0.7
0.6
0.5
0.4
0
5
10
15
20
25
30
35
Number of sensors

B

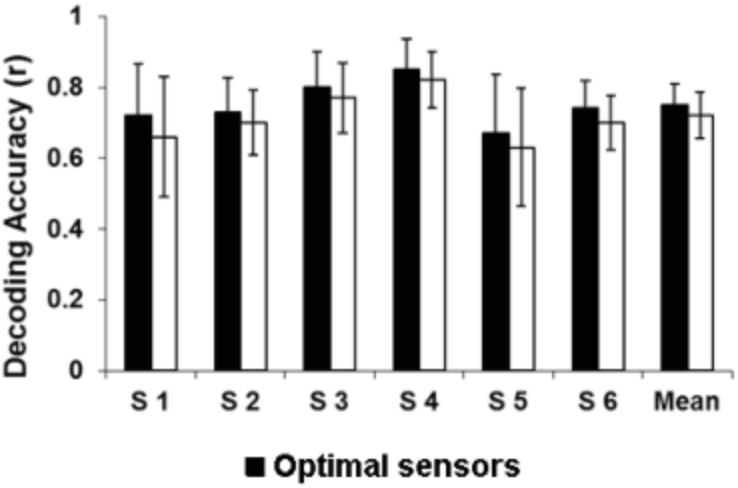
Decoding Accuracy (r)
1
0.8
0.6
0.4
0.2
0
S 1
S 2
S 3
S 4
S 5
S 6
Mean
Optimal sensors
Plateau sensors

C

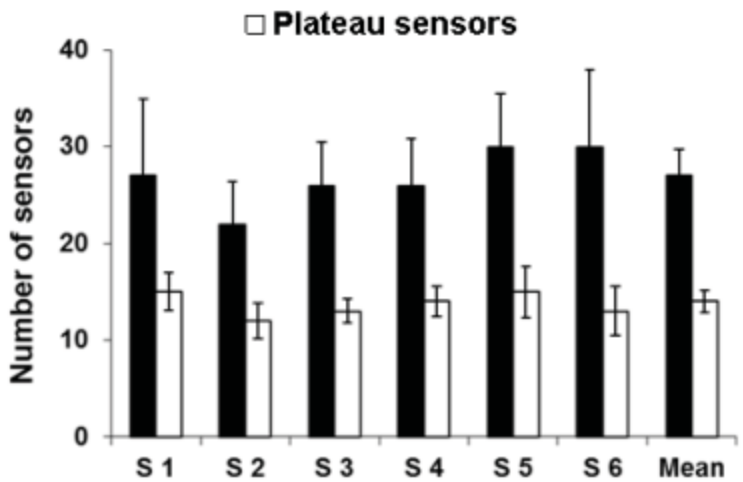
Number of sensors
40
30
20
10
0
S 1
S 2
S 3
S 4
S 5
S 6
Mean

A

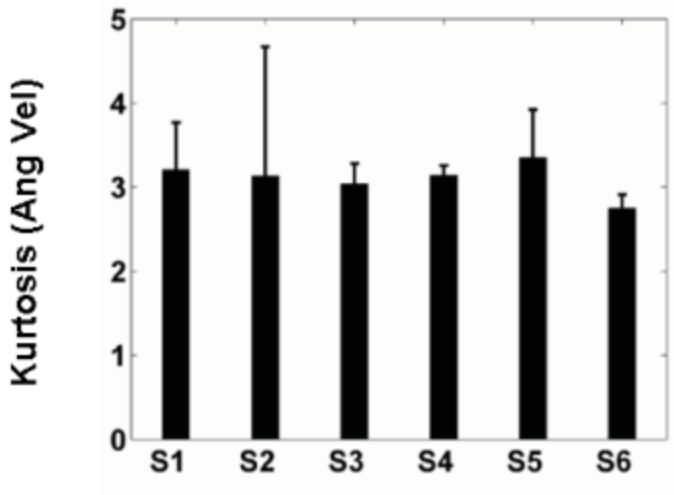
Kurtosis (Ang Vel)
5
4
3
2
1
0
S1
S2
S3
S4
S5
S6

B

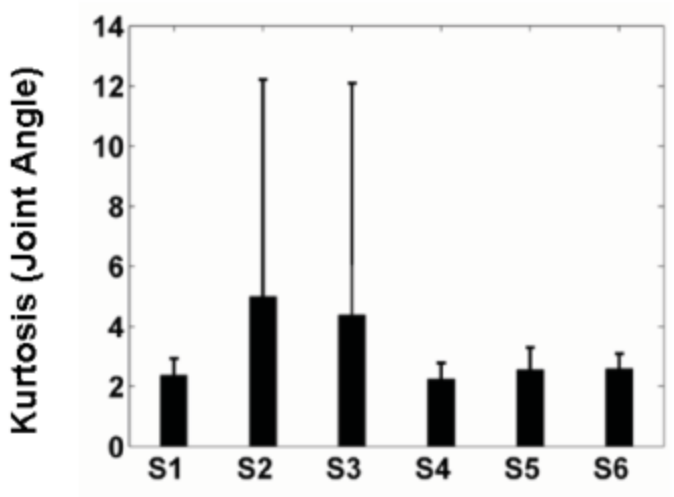
Kurtosis (Joint Angle)
14
12
10
8
6
4
2
0
S1
S2
S3
S4
S5
S6

C

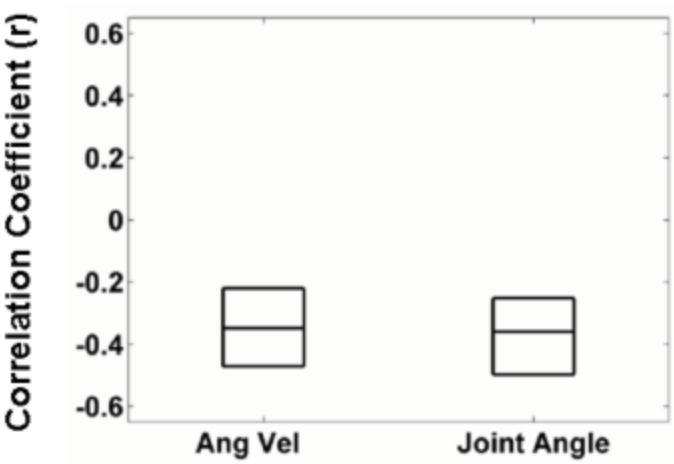
Correlation Coefficient (r)
0.6
0.4
0.2
0
-0.2
-0.4
-0.6
Ang Vel
Joint Angle

Table 1: Comparison of decoding results in nonhuman primates with the current human study.

Spikes			EEG					
Monkey 1			Subject 4 (Best)		Subject 5 (Worst)		Mean (6 subjects)	
Ankle	r	SNR	r	SNR	r	SNR	r	SNR
X	0.79 ± 0.09	4.08 ± 1.8	0.81 ± 0.02	4.71 ± 0.67	0.59 ± 0.12	1.43 ± 1.74	0.58 ± 0.17	1.9 ± 1.74
Y	0.86 ± 0.11	6.25 ± 2.66	0.92 ± 0.009	8.13 ± 0.48	0.71 ± 0.17	2.64 ± 3.34	0.8 ± 0.08	4.84 ± 2.11
Z	0.44 ± 0.15	-0.2 ± 1.48	0.92 ± 0.009	8.03 ± 0.4	0.73 ± 0.11	3.04 ± 2.38	0.76 ± 0.1	4.27 ± 2.19
Joint Angle	N/A	N/A	0.87 ± 0.01	6.1 ± 0.59	0.68 ± 0.11	2.19 ± 2.44	0.68 ± 0.08	2.81 ± 1.16
Ang Vel	N/A	N/A	0.81 ± 0.03	4.54 ± 0.7	0.67 ± 0.08	2.11 ± 2.04	0.71 ± 0.08	3.26 ± 1.63
Knee	r	SNR	r	SNR	r	SNR	r	SNR
X	0.66 ± 0.14	1.96 ± 1.84	0.6 ± 0.06	1.9 ± 0.66	0.4 ± 0.07	0.15 ± 0.87	0.67 ± 0.16	2.22 ± 1.43
Y	0.79 ± 0.13	4.28 ± 2.02	0.9 ± 0.01	7.21 ± 0.6	0.71 ± 0.14	2.64 ± 2.61	0.82 ± 0.07	5.11 ± 1.98
Z	0.39 ± 0.13	-0.52 ± 1.36	0.91 ± 0.005	7.71 ± 0.51	0.74 ± 0.08	3.12 ± 1.92	0.8 ± 0.07	4.73 ± 1.8
Joint Angle	0.84 ± 0.07	5.29 ± 2.06	0.92 ± 0.01	8.41 ± 0.6	0.75 ± 0.1	3.29 ± 2.2	0.85 ± 0.04	5.95 ± 1.35
Ang Vel	N/A	N/A	0.9 ± 0.02	7.16 ± 0.86	0.81 ± 0.08	4.62 ± 2.2	0.84 ± 0.05	5.75 ± 1.66
Hip	r	SNR	r	SNR	r	SNR	r	SNR
X	0.6 ± 0.14	1.15 ± 1.71	0.76 ± 0.04	3.68 ± 0.68	0.57 ± 0.08	1.05 ± 1.5	0.77 ± 0.11	3.54 ± 1.47
Y	0.66 ± 0.14	1.97 ± 1.92	0.82 ± 0.01	4.86 ± 0.31	0.72 ± 0.07	2.84 ± 1.77	0.7 ± 0.1	2.97 ± 1.44
Z	0.56 ± 0.13	0.66 ± 1.75	0.85 ± 0.02	5.8 ± 0.72	0.71 ± 0.1	2.9 ± 1.99	0.81 ± 0.06	5 ± 1.43
Joint Angle	0.73 ± 0.11	2.95 ± 1.95	0.9 ± 0.01	7.29 ± 0.6	0.68 ± 0.16	2.11 ± 3.16	0.81 ± 0.07	5.03 ± 1.79
Ang Vel	N/A	N/A	0.88 ± 0.006	6.56 ± 0.31	0.71 ± 0.13	2.77 ± 2.5	0.8 ± 0.09	4.82 ± 2.3

Correlation coefficient (r) and SNR (dB) for the prediction of different walking parameters for Monkey 1 (Fitzsimmons et al. (2009)), the best (S4) and worst (S5) decoded subjects, and for the mean across the 6 subjects in the current study. The numbers represent mean ± standard deviation.

Table 2: Comparison of decoding results between precision and natural walking.

	Subject 4 (Precision walking)		Subject 4 (Natural walking)		Subject 5 (Precision walking)		Subject 5 (Natural walking)	
Ankle	**r**	**SNR**	**r**	**SNR**	**r**	**SNR**	**r**	**SNR**
X	0.81 ± 0.02	4.71 ± 0.67	0.47 ± 0.17	-1.55 ± 4.51	0.59 ± 0.12	1.43 ± 1.74	0.77 ± 0.03	3.84 ± 0.65
Y	0.92 ± 0.009	8.13 ± 0.48	0.75 ± 0.16	3.26 ± 3.45	0.71 ± 0.17	2.64 ± 3.34	0.83 ± 0.03	4.99 ± 0.84
Z	0.92 ± 0.009	8.03 ± 0.4	0.81 ± 0.11	4.58 ± 2.99	0.73 ± 0.11	3.04 ± 2.38	0.86 ± 0.02	5.69 ± 0.55
Joint Angle	0.87 ± 0.01	6.1 ± 0.59	0.68 ± 0.13	1.79 ± 3	0.68 ± 0.11	2.19 ± 2.44	0.84 ± 0.02	5.43 ± 0.64
Ang Vel	0.81 ± 0.03	4.54 ± 0.7	0.75 ± 0.07	3.52 ± 1.43	0.67 ± 0.08	2.11 ± 2.04	0.82 ± 0.02	4.74 ± 0.68
Knee	**r**	**SNR**	**r**	**SNR**	**r**	**SNR**	**r**	**SNR**
X	0.6 ± 0.06	1.9 ± 0.66	0.37 ± 0.11	-1.03 ± 3.02	0.4 ± 0.07	0.15 ± 0.87	0.36 ± 0.04	0.04 ± 0.62
Y	0.9 ± 0.01	7.21 ± 0.6	0.74 ± 0.07	2.45 ± 2.02	0.71 ± 0.14	2.64 ± 2.61	0.82 ± 0.04	4.97 ± 1.07
Z	0.91 ± 0.005	7.71 ± 0.51	0.76 ± 0.09	3.49 ± 2.44	0.74 ± 0.08	3.12 ± 1.92	0.85 ± 0.02	5.63 ± 0.76
Joint Angle	0.92 ± 0.01	8.41 ± 0.6	0.82 ± 0.1	4.82 ± 2.82	0.75 ± 0.1	3.29 ± 2.2	0.86 ± 0.02	5.93 ± 0.59
Ang Vel	0.9 ± 0.02	7.16 ± 0.86	0.84 ± 0.04	5.23 ± 1.42	0.81 ± 0.08	4.62 ± 2.2	0.87 ± 0.02	6.22 ± 0.71
Hip	**r**	**SNR**	**r**	**SNR**	**r**	**SNR**	**r**	**SNR**
X	0.76 ± 0.04	3.68 ± 0.68	0.64 ± 0.15	0.79 ± 3.54	0.57 ± 0.08	1.05 ± 1.5	0.67 ± 0.03	2.38 ± 0.39
Y	0.82 ± 0.01	4.86 ± 0.31	0.71 ± 0.19	2.3 ± 4.05	0.72 ± 0.07	2.84 ± 1.77	0.79 ± 0.02	4.17 ± 0.61
Z	0.85 ± 0.02	5.8 ± 0.72	0.81 ± 0.09	4.64 ± 2.02	0.71 ± 0.1	2.9 ± 1.99	0.83 ± 0.03	5.1 ± 0.79
Joint Angle	0.9 ± 0.01	7.29 ± 0.6	0.82 ± 0.07	4.72 ± 1.93	0.68 ± 0.16	2.11 ± 3.16	0.81 ± 0.04	4.71 ± 1.04
Ang Vel	0.88 ± 0.006	6.56 ± 0.31	0.66 ± 0.14	1.27 ± 3.02	0.71 ± 0.13	2.77 ± 2.5	0.81 ± 0.03	4.74 ± 0.72

Correlation coefficient (r) and SNR (dB) for the prediction of different walking parameters for the best (S4) and worst (S5) decoded subjects under precision and natural walking. The numbers represent mean ± standard deviation.

Table 3: Comparison of decoding accuracy (r) and weights between decoding with and without eye- electrode.

	Subject 1		Subject 2		Subject 3		Subject 4		Subject 5		Subject 6	
Ankle	%weight	%r	%weight	%r	%weight	%r	%weight	%r	%weight	%r	%weight	%r
X	0.1	0	0.1	2.9	0.08	-1.4	0.08	0	0.07	3.5	0.05	3.1
Y	0.03	-1.2	0.05	5.1	0.07	-1.1	0.09	0	0.06	2.8	0.07	-1.1
Z	0.05	0	28.7	9.6	0.18	0	0.05	0	0.06	1.3	0.06	0
Joint Angle	0.1	0	0.09	0	0.24	0	0.12	-1.21	0.03	-1.4	0.06	0
Ang Vel	0.04	0	0.09	-4.4	0.09	0	0.1	-1.1	0.04	0	0.12	0
Knee	%weight	%r	%weight	%r	%weight	%r	%weight	%r	%weight	%r	%weight	%r
X	0.07	0	0.14	-1.2	0.12	-1.35	0.08	-1.6	0.05	0	0.06	1.75
Y	0.07	0	0.11	-6	0.07	-1	0.04	-1	0.04	2.8	0.04	0
Z	0.06	0	0.13	-2.3	0.06	-1.3	0.09	0	0.03	1.3	0.06	0
Joint Angle	0.04	1.2	0.08	-1.1	0.04	-1.1	0.09	0	0.04	0	0.02	0
Ang Vel	0.1	0	0.13	-2.2	0.08	-1.1	0.11	-1	0.07	1.35	0.03	0
Hip	%weight	%r	%weight	%r	%weight	%r	%weight	%r	%weight	%r	%weight	%r
X	0.05	-1.2	0.13	-4.8	0.08	0	0.04	-1.2	0.06	1.78	0.04	0
Y	0.05	-1.4	0.1	0	0.04	-1.23	0.09	0	0.05	0	0.12	-1.88
Z	0.07	-1.2	0.11	0	0.04	0	0.04	-2.2	0.08	1.4	0.05	0
Joint Angle	0.05	0	0.07	-4.7	0.06	0	0.04	-1.1	0.02	1.4	0.04	0
Ang Vel	0.06	0	0.09	-7.5	0.08	-1	0.06	0	0.05	3	0.04	0

The difference in % between correlation coefficient (r) and the ratio between weights for the prediction of different walking parameters for the six subjects decoded under precision walking with and without eye-electrode are shown in table 3. Positive values mean an increase of r and weight with eye-electrode, while negative values mean a decrease of r and weight with eye-electrode.